Isolated Nuclei Stiffen in Response to Low Intensity Vibration

Newberg J[1], Schimpf J[2], Woods K[1], Loisate S[1], Davis P H[2], Uzer G[1†]

[1]Mechanical and Biomedical Engineering, Boise State University

[2]Micron School of Material Science, Boise State University

[†] Corresponding Author

Running title: Isolated Nuclei Stiffen in Response to Low Intensity Vibration

Funding support: NIH R01AG059923, and 5P2CHD086843-03, P20GM109095, P20GM103408, NSF 1929188 and NASA ISGC NNX15AI04H.

[†] Corresponding author:

Gunes Uzer PhD

Boise State University

Department of Mechanical & Biomedical Engineering

1910 University Drive, MS-2085

Boise, ID 83725-2085

Ph. (208) 426-4461

Email: gunesuzer@boisestate.edu

ABSTRACT

The nucleus, central to all cellular activity, relies on both direct mechanical input and its molecular transducers to sense and respond to external stimuli. While it has been shown that isolated nuclei can adapt to applied force *ex vivo*, the mechanisms governing nuclear mechanoadaptation in response to physiologic forces *in vivo* remain unclear. To investigate nuclear mechanoadaptation in cells, we developed an atomic force microscopy (AFM) based procedure to probe live nuclei isolated from mesenchymal stem cells (MSCs) following the application of low intensity vibration (LIV) to determine whether nuclear stiffness increases as a result of LIV. Results indicated that isolated nuclei were, on average, 30% softer than nuclei tested within intact MSCs prior to LIV. When the nucleus was isolated following LIV (0.7g, 90Hz, 20min) applied four times (4x) separated by 1h intervals, stiffness of isolated nuclei increased 75% compared to non-LIV controls. LIV-induced nuclear stiffening required functional Linker of Nucleoskeleton and Cytoskeleton (LINC) complex, but was not accompanied by increased levels of the nuclear envelope proteins LaminA/C or Sun-2. While depleting LaminA/C or Sun-1&2 resulted in either a 47% or 39% *increased* heterochromatin to nuclear area ratio in isolated nuclei, the heterochromatin to nuclear area ratio was *decreased* by 25% in LIV-treated nuclei compared to controls, indicating LIV-induced changes in the chromatin structure. Overall, our findings indicate that increased apparent cell stiffness in response to exogenous mechanical challenge of MSCs in the form of LIV is in part retained by increased nuclear stiffness and changes in chromatin structure.

Key words: Mesenchymal Stem Cells, Nucleus, LINC complex, Low Intensity Vibration

45 **Introduction**

46 Influence of the mechanical environment is perhaps most evident in resident stem cells which
47 need to remodel their respective tissues in response to changing tissue mechanics (Rando and
48 Ambrosio, 2018). For example, mesenchymal stem cells (MSCs) that replace and regenerate
49 bone, when seeded into substrates with increasing stiffness tend to differentiate into bone
50 lineage (Sun et al., 2018) through regulation of actin cytoskeleton dynamics and intra-nuclear
51 Lamina (Buxboim et al., 2014; Swift et al., 2013). While cell structural changes and signaling
52 events that take place within the focal adhesions and cytoskeletal compartments in response to
53 environmental mechanical challenges are well studied (Lessey et al., 2012) the changes that
54 occur inside the nucleus in response to physiological forces are less understood.
55
56 Dynamic forces applied to the exterior of the cell propagate through the cell via focal adhesions
57 and cytoskeletal components, and reach the structural components at the outer and inner
58 membranes of the nucleus, regulating nuclear structure (Martins et al., 2012). The nucleus is
59 integrated within the cell structure through direct connections with cytoskeletal elements
60 (Lombardi et al., 2011) through the LINC complexes (Linker of Nucleoskeleton and
61 Cytoskeleton) composed of Nesprin and Sun subunits (Crisp et al., 2006). When forces are
62 applied directly to the nucleus through LINC connections *ex vivo*, resulting in large strain
63 deformations, nuclei stiffen via tyrosine phosphorylation of emerin (Guilluy et al., 2014)
64 suggesting the nucleus is an active contributor to mechanotransduction. The nucleus also
65 undergo structural re-organization in response to F-actin contractility by recruiting LINC
66 complexes to apical stress fibers, leading to the accumulation of nuclear lamina element

67 LaminA/C as well as changes in chromatin density under these stress fibers (Versaevel et al.,
68 2014). At the level of DNA, forces applied at the cell membrane propagate through the
69 cytoskeletal actin framework to cause deformations in chromatin (Tajik et al., 2016) and alter
70 heterochromatin dynamics (Le et al., 2016). Nuclear stiffness is also in-part managed by the
71 same toolset, Nesprins are anchored to the inner nuclear membrane through Sun-1&2 proteins
72 that directly interact with structural elements such as nuclear pore complexes and LaminA/C
73 (Hodzic et al., 2004; Padmakumar et al., 2005). Both Sun-1&2 and LaminA/C, play key roles in
74 the structural integrity of the cell nucleus (Neelam et al., 2015). Inside the nucleus, both
75 LaminA/C and chromatin have been shown to play independent roles in regulating nuclear
76 mechanics (Stephens et al., 2017).
77
78 The elastic modulus of a cell nucleus can also be a marker of cell health. For example, it has
79 been reported that the nuclei of Hepatitis C-infected cells are significantly softer than healthy
80 controls, which was paralleled by downregulation of LaminA/C paired with upregulation of β-
81 actin (Balakrishnan et al., 2019). Likewise, breast cancer cells exhibit large decreases in nuclear
82 stiffness relative to healthy controls, showing downregulation of both LaminA/C and Sun-1&2
83 (Matsumoto et al., 2015). Furthermore, coinciding research showed chromatin decondensation
84 as an additional component in highly metastatic cancer cells (Khan et al., 2018).
85
86 The nuclear envelope is subject to F-actin generated tension through LINC complex connections
87 (Arsenovic et al., 2016). While cyto-mechanical forces can be generated in a multitude of ways,
88 our group has focused on low intensity vibrations (LIV). LIV is a mechanical regime modeled

89 after physiological, high frequency muscle contractions (Ozcivici et al., 2010). In MSCs, LIV
90 promotes proliferation and osteogenic differentiation (Uzer et al., 2013) as well as increasing
91 cell contractility by promoting GTP-bound RhoA (Ras homolog family member A)(Uzer et al.,
92 2015). While we have further reported that daily LIV application up to 14 days increases
93 stiffness of F-actin struts and results in increased mRNA expression of the LINC-related genes
94 Nesprin-1&2, Sun-1&2, and LaminA/C in MSCs (Pongkitwitoon et al., 2016), the role of short
95 term acute LIV application on the nuclear structural properties remains unknown.
96
97 Therefore, in this study we utilized AFM (atomic force microscopy) based nanoindentation
98 measurements, immunostaining, and quantification of nuclear structural proteins to probe
99 nuclear mechanical properties and morphology in response to acute bouts of LIV. We
100 hypothesized that application of LIV to MSCs will increase nuclear stiffness.
101
102 **Results**
103 *Cytoskeletal tension alters nuclear shape*
104 We first investigated nuclear shape before and after our nuclear isolation protocol. **Fig. 1a**
105 shows intact MSC (top) and isolated nuclei (bottom) after Hoechst 33342 staining to label DNA.
106 As shown in **Fig. 1a**, the areas of isolated nuclei were visibly smaller than that of nuclei inside
107 intact MSCs. As shown in Figures **1b** & **S1,** DNA structure and LaminA/AC organization remained
108 intact within the isolated nuclei. We next evaluated the relative circularity of intact MSC nuclei
109 versus isolated nuclei by measuring their XY (top view), XZ (side view), and YZ (side view) areas
110 and combining these three-dimensional measurements to evaluate overall sphericity (**Fig. 1c**).

111 In the XY plane (i.e., the horizontal plane of the cell culture dish), intact and isolated nuclei
112 showed no circularity differences. The isolated nuclei were 52% and 45% more circular than
113 the nuclei of intact MSCs in the vertical XZ and YZ planes, respectively ($p<.001$). Combining the
114 circularity values for each plane, the average circularity (i.e., sphericity) of the isolated nuclei
115 was 0.809, which was significantly higher than that of the intact MSC nuclei (0.612, $p<.001$).
116 Measures of nuclear height and volume (Figures **1d** & **1e**) showed that following nuclear
117 isolation, height approximately doubled, increasing by 105% ($p<.001$) , while overall volume
118 decreased by 44% ($p<.001$).
119
120 *Nucleus significantly contributes to AFM-measured MSC stiffness*
121 To investigate the mechanical properties of the nucleus, AFM-based nanoindentation was used
122 to measure and compare elastic moduli values of intact MSC nuclei and isolated cell nuclei
123 (**Fig.2a**). Prior to testing, tipless AFM MLCT-D probes were functionalized with 10 µm glass
124 beads (Thermo Scientific 9010, Figures **2b** & **S2a**). Nuclei of intact MSCs and isolated nuclei
125 were probed at the nuclear center visible in the XY plane (**Fig.2a**). To test whether fixation
126 methods preserve nuclear stiffness, isolated nuclei were fixed in 2% paraformaldehyde (PFA)
127 for 10 minutes and compared to untreated live controls. As shown in **Fig. 2c**, the results
128 indicated a 4-fold increase in stiffness between PFA-treated and control nuclei ($p<.01$).
129
130 With fixation having been shown to significantly impact measured stiffness, we next
131 determined the time window during which stiffness of live cell nuclei remains stable. Moduli of
132 isolated live nuclei were measured across 3 one-hour time blocks, namely 0 to 1 hour, 1 to 2

133 hours, and 2 to 3 hours following isolation. **Fig. 2d** indicates that no change was observed in the
134 mechanical properties of isolated nuclei up to two hours post-isolation, after which a large
135 spike in stiffness occurred 2-3 hours following isolation (+406%, $p<.01$). Accordingly, a one hour
136 post-isolation window for AFM-based nanoindentation testing was deemed safe and unlikely to
137 skew the results. With this protocol established, we compared the stiffness of intact MSC nuclei
138 (tested in the center of the nucleus) versus isolated nuclei within 1 hr of isolation. As shown in
139 **Fig. 2e**, the average modulus of the isolated nuclei (1.5 kPa) was significantly softer than that
140 obtained for the nuclei of intact MSCs (2.19 kPa, $p<.05$), indicating that the nucleus itself
141 accounted for 69.7% of the overall MSC stiffness.
142
143 *Disruption of LaminA/C decreases nuclear stiffness and increases heterochromatin area in*
144 *isolated nuclei*
145 We next probed the effects of depleting known structural members in the nuclear membrane:
146 Nuclear Lamina element, LaminA/C, and LINC complex elements Sun-1 and Sun-2 (**Fig. 3a**).
147 Following siRNA depletion of LaminA/C (siLmn), co-depletion of Sun-1&2 (siSun), or control
148 siRNA (siCntrl), groups were divided into either intact MSCs or underwent the nuclear isolation
149 protocol. The siLmn group showed a 63.2% and 49.7% modulus decrease in intact MSCs ($p<.05$)
150 and isolated nuclei ($p<.01$), respectively (**Fig. 3b**). Likewise, siSun treatment resulted in 50.7%
151 and 27.7% decreased modulus for intact MSCs and isolated nuclei, respectively, but changes
152 remained not significant compared to siCntrl (**Fig. 3b**).
153

154 Hoechst staining of DNA can be used to identify heterochromatin (Imai et al., 2017). We
155 therefore quantified average heterochromatin size following LaminA/C or Sun-1&2 depletion
156 using Hoechst 33342 and epifluorescence imaging (**Fig. 3c**). As shown in **Fig. 3d,** nuclear area
157 increased 33% in siLmn MSCs (p<.001), but not in siSun MSCs. While overall nuclear area was
158 smaller in isolated nuclei, no differences were observed in nuclear area between controls and
159 isolated nuclei subjected to siRNA treatments (**Fig. 3d**). Combining the results presented in **Fig.**
160 **3c** and **3d**, the ratio of heterochromatin area to nuclear area was calculated to investigate
161 possible changes in the heterochromatin condensation. As shown in **Fig. 3e**, measurement of
162 the heterochromatin to nuclear area ratio in intact MSCs showed no changes between the
163 control and siRNA-treated groups. In contrast, a comparison of the heterochromatin to nuclear
164 area ratio of isolated nuclei showed significantly larger ratios compared to siCntrl for both the
165 siLmn group (47.2% increase, p<.001) and the siSun group (39.1% increase p<.001).
166
167 *Low Intensity Vibration (LIV) stiffens MSCs and isolated nuclei*
168 To evaluate nuclear mechanics following LIV, we subjected intact MSCs to either 2x or 4x low
169 intensity vibration protocols. The LIV regimen is illustrated in **Fig. 4a**. As shown in **Figures 4b**
170 and **4c**, following 2x LIV, intact MSCs showed a 71% increase in stiffness (p<.05), but there was
171 no significant change in nuclear stiffness for isolated nuclei that underwent the same vibration
172 protocol. In contrast, application of 4x LIV significantly increased the elastic modulus of both
173 intact MSCs (419% increase, p<.001) and isolated nuclei (75%, p<.05).
174

175 To investigate the source of the observed changes in mechanical properties following LIV, the
176 cytoplasmic and nuclear compartments were probed via western blotting. LaminA/C and Sun-2
177 protein levels following the 4x LIV protocol was quantified to test whether LIV results in
178 upregulation of either protein. These protein levels were then compared to PARP and GAPDH
179 as control markers. **Fig. 4d** shows no significant differences were observed in LaminA/C or Sun-
180 2 protein levels, either in the cytoplasmic or nuclear fractions, following a 4x LIV protocol.
181
182 *Isolated nuclei maintain heterochromatin area after vibration*
183 As LIV-induced stiffness increase was not accompanied by changes in LaminA/C or Sun-2
184 proteins, we probed possible changes in heterochromatin by comparing the heterochromatin
185 to nuclear area ratio between 4x LIV and control samples for intact and isolated nuclei (**Fig 5a**).
186 As shown in **Fig.5b**, intact MSCs subjected to 4x LIV showed no difference in nuclear area
187 compared to controls. Likewise, there was no difference in nuclear area between isolated nuclei
188 subjected to 4x LIV and the corresponding controls. As shown in **Fig.5c**, intact MSCs subject to
189 4xX LIV showed no difference in heterochromatin to nuclear area ratio compared to controls.
190 In contrast to LaminA/C and Sun-1&2 depleted nuclei (**Fig.3e**) which showed higher chromatin
191 to nuclear area ratio compared to control siRNA, isolated nuclei subjected to 4x LIV, showed a
192 25.4% decrease in chromatin to nuclear area ratio compared to non-LIV controls ($p<.05$).
193
194 *LINC function is required for LIV-induced nuclear stiffening*
195 To test the requirement of cytoskeletal connections to the nucleus in the LIV response, we used
196 LINC-compromised MSCs (referred to as +KASH). As depicted in **Fig.6a**, using previously

197 established methods (Uzer et al., 2015), LINC complex function was disrupted by
198 overexpressing a dominant negative form of the Nesprin KASH domain (pCDH-EF1-MSC1-puro-
199 mCherry-Nesprin-1αKASH), which serves to disrupt the connection between Nesprin and Sun
200 proteins via competitive binding to Sun proteins. Compared to empty control plasmid (pCDH-
201 EF1-MSC1-puro-mCherry, referred to as mCherry), LINC-disrupted intact cells and isolated
202 nuclei did not show any changes in stiffness (**Fig.S3**). As shown in Figures **6b** and **6c**, comparing
203 intact MSC and isolated nuclear stiffness with or without 4x LIV showed no significant changes
204 in elastic modulus between non-vibrated and vibrated MSCs with +KASH insertion.
205
206 **Discussion**
207 Here we investigated the effects of a low magnitude, low intensity vibration (LIV) protocol on
208 mesenchymal stem cell nuclei mechanical properties. Our results show that nucleus retains
209 about 70% of its mechanical properties when isolated. Further the nucleus responds to low
210 intensity vibration by increasing its apparent stiffness, not due to an increase in LaminA/C or
211 Sun-2 protein amounts, but instead perhaps through changes in chromatin organization.
212
213 When cyto-mechanical forces that keep nucleus elongated was removed during nuclear
214 isolation, isolated nuclei changed shape from 60% to 80% sphericity (**Fig. 1c**). We also observed
215 a reduction in nuclear volume post isolation. While cytoskeletal force may, in part, account for
216 the observed volume changes, nuclear volume depends on other factors including changes in
217 pH, salt conditions, and temperature (Chan et al., 2017). Additionally, loss of protein structures
218 during nuclear isolation has been reported (Paine et al., 1983). Although a potential limitation

219 exist in the isolation technique, we confirmed changes in isolated nuclei stiffness via AFM-based
220 measurements of elastic modulus (**Fig. 4c**).
221
222 When MSCs treated with siRNA protocols, both intact MSC and isolated nuclei modulus were
223 consistently lower than non-siRNA counterparts (**Fig. 3b**), similar batch effects are also seen in
224 KASH inserted MSCs **(Fig.6**). Increased stiffness of KASH inserted MSCs is probably due to
225 extended culturing period during puromycin mediated selection process (see supplementary
226 methods) as later passage MSCs were stiffer (**Fig. S4**) While this global shift in stiffness under
227 siRNA treatment and plasmid overexpression remains as a limitation, in agreement with
228 literature, depletion of LaminA/C showed significantly lower modulus compared to control
229 siRNA (Lammerding et al., 2006). Softer nuclei, due to LaminA/C depletion also resulted in
230 increased nuclear area (**Fig.3d**). This softening and concomitant increased nuclear area points
231 to a weakening of nuclear structure. As expected, when Sun-1&2 were co-depleted, we did not
232 observe any changes in the nuclear area of intact MSCs (**Fig.3d**), owing to an absence of
233 cytoskeletal connections (Uzer et al., 2018). Following nuclear isolation (i.e. in the absence of
234 cytoskeletal connections), both LaminA/C and Sun-1&2 depleted nuclei showed large increases
235 in heterochromatin area. This observation suggests that in the absence of cytoskeletal
236 constraints, nuclear Lamina and Sun proteins can have secondary effects on heterochromatin
237 structure.
238
239 Acute application of LIV caused a significant increase in stiffness for both intact MSC nuclei and
240 isolated nuclei (**Fig.4b**), suggesting that the changes in cellular stiffness and cytoskeletal tension

241 (Pagnotti et al., 2019) in response to LIV were in-part retained by nucleus as increased stiffness
242 even after nuclear isolation protocol. Though the stiffness was increased, there were no short-
243 term changes in the levels LaminA/C and Sun-2 (**Fig.4c**). As the LIV-induced stiffening of
244 isolated nuclei were lower than that of intact MSCs, our findings suggests other mechanisms
245 responsible for MSC stiffening in response to LIV, such as the cytoskeletal connections to the
246 nucleus. Additionally, disrupting the LINC complex connections and applying the same 4x LIV
247 protocol showed no changes in elastic modulus. This further suggests that cytoskeletal
248 components contribute to the overall stiffening response of both intact MSCs and isolated
249 nuclei.
250
251 Image analysis indicated a retention of chromatin to nuclear area ratio in LIV treated MSCs post
252 nuclear isolation (**Fig. 5c**). When cytoskeletal constraints were removed during nuclear
253 isolation, nuclear to chromatin area ratio was increased in both control and LIV treated MSC
254 nuclei, although nuclei subjected to 4x LIV showed significantly smaller, or more condensed
255 heterochromatin compared to controls. These findings show that the effects of LIV were
256 maintained by chromatin after the nucleus was mechanically separated from the cytoskeleton.
257 While the mechanism by which this happens is again outside the scope of this current work,
258 differences in DNA organization between isolated nuclei subject to LIV vs non-LIV counterparts
259 may contribute to the increased stiffening of the nucleus (Stephens et al., 2018), suggesting
260 that DNA organization plays a role in LIV-induced mechanoadaptation. Consequently LIV-
261 induced decrease in the heterochromatin area post-isolation can potentially be a marker of

262 altered gene access in response to environmental factors (Miroshnikova et al., 2017; Rubin et
263 al., 2018).
264
265 Until now, it was previously unknown whether the nucleus responds to low intensity vibration
266 in living cells. Our findings show that the nucleus is a mechanoresponsive element and
267 responds to low intensity vibration by increasing its stiffness as confirmed by elastic modulus
268 measurements. The mechanism(s) responsible for this stiffness regulation are not fully known,
269 but our findings suggest that chromatin structure and cytoskeletal connections likely play a role
270 in nuclear stiffening in response to LIV. Thus future studies aimed at understanding how LIV and
271 other forms of mechanical signals regulate the mechanics of nucleoskeletal and chromatin
272 structures may uncover new mechanisms by which forces regulate gene expression and cellular
273 decisions.
274
275 **Materials and Methods**
276 *Cell Culture*
277 Primary mouse mesenchymal stem cells (MSCs) were extracted as previously described (Case et
278 al., 2010; Peister et al., 2004). MSCs between passages seven (P8) and eleven (P11) were used
279 during experiments for consistency, as higher passages showed significantly higher moduli, **Fig.**
280 **S4**. For sub-culturing, cells were re-plated at a density of 1,800/cm^2 and maintained in IMDM
281 (12440053, GIBGO) supplemented with 10% FCS (S11950H, Atlanta Biologicals) and 1%
282 Pen/Strep. For whole cell experiments, MSCs were plated into 35 mm diameter dishes prior to
283 application of LIV. For nuclear extraction experiments, cells were maintained in 55 cm^2 culture

284 dishes until 80% confluency (approximately 1.5 – 2 million cells) prior to application of LIV.
285 Transfections and siRNA were applied 72 hr prior to isolation protocols (see Supplementary
286 Methods).
287
288 *Nuclear Isolation*
289 MSCs were gently removed from plates by scraping in 9 mL of 1x PBS and centrifuged at 1100
290 RPM at 4°C (Beckman Coulter Allegra X-30R). MSCs were then gently suspended with 500 µL
291 hypotonic buffer (0.33 M sucrose, 10 mM HEPES, pH 7.4, 1 mM $MgCl_2$, 0.5% w/v Saponin) and
292 centrifuged twice more at 3000 RPM, 4°C for 10 minutes (Beckman Coulter Microfuge 20R
293 Centrifuge). For western blots, the cytoplasmic fraction (supernatant) and nuclei (pellet) were
294 saved separately. For AFM experiments, the cytoplasmic supernatant was aspirated and nuclei
295 were resuspended in 100 µL of hypotonic buffer (Buffer A). To gently separate cytoplasmic
296 debris from nuclei, the resuspended pellet was added to 400 µL of Percoll (Sigma Aldrich) +
297 (81% w/v Percoll, Buffer A) and centrifuged at 10,000 RPM, 4°C for 10 minutes. Isolated nuclei
298 were then plated in a 0.01% poly-L-lysine coated 35 mm cell culture dish and incubated for 25
299 minutes for adherence.
300
301 *Low Intensity Vibration (LIV) Protocol*
302 Vibrations were applied to MSCs at a peak magnitudes of 0.7 g at 90 Hz for 20 minutes at room
303 temperature(Sen et al., 2011). Controls were handled the same way, but the LIV device was not
304 turned on. LIV was applied as either, two (2x) or four (4x), twenty-minute vibration periods with
305 one-hour rest in-between.

306 *Atomic Force Microscopy (AFM)*

307 Force-displacement curves for both intact MSC nuclei and isolated nuclei acquired using a
308 Bruker Dimension FastScan AFM. Tipless MLCT-D probes (0.03 N/m spring constant) were
309 functionalized with 10 µm diameter borosilicate glass beads (Thermo Scientific 9010, 10.0 ± 1.0
310 µm NIST-traceable 9000 Series Glass Particle Standards) prior to AFM experiments using UV-
311 curable Norland Optical Adhesive 61 (**Fig. S2a**). To ensure accurate force measurements, each
312 probe must be individually calibrated. Accordingly, a thermal tune was conducted on each
313 probe immediately prior to use to determine its spring constant and deflection sensitivity (**Fig.**
314 **S2b**). MSCs and nuclei were located using the AFM's optical microscope and engaged on using a
315 minimal force setpoint (2-3 nN) to minimize damage prior to testing. Ramps were performed
316 over the approximate center of each nucleus for all samples. Force curve ramping was
317 performed at a rate of 2 µm/sec over 2 µm total travel (1 µm approach, 1 µm retract; **Fig. S2c**).
318 Three replicate force-displacement curves were acquired and saved for each nucleus tested,
319 with at least 3 seconds of rest between conducting each test. Measurements that showed
320 minimal contact with the nucleus were discarded and performed again to ensure an adequate
321 depth of probing.

322

323 Measured force-displacement curves were analyzed assuming Hertzian (spherical contact)
324 mechanics(Guo et al., 2012), employing Bruker's Nanoscope Analysis software package to
325 obtain the elastic modulus of the samples. Accordingly, MSC and nuclear stiffness were
326 quantified in Nanoscope Analysis using a best-fit curve to a Hertzian model. The point of initial
327 contact was visually selected, and the curve was analyzed until the R^2 value was greater than

328 0.95 ($p<0.05$). The modulus of each individual sample (i.e., intact MSC or isolated nucleus) was
329 reported as the average of three consecutive measurements. Group averages were then
330 obtained from the average values for the individual samples.
331
332 *Statistical Analysis*
333 Unless indicated otherwise in figure legends, results are expressed as mean ± standard error of
334 the mean throughout. All experiments were replicated at least three times to ensure
335 reproducibility. Densitometry and other analyses were performed on at least three
336 independent experiments. As we previously reported (Uzer et. al 2018, Touchstone et al. 2019),
337 for western blot data, differences between treatments within each biological replicate were
338 assumed to follow a normal distribution due to large mean sample; thus for these comparisons,
339 we have used two-tailed un-paired T-tests (Figure 4d). For other comparisons, we used a non-
340 parametric two-tailed Mann-Whitney U-test (Figures 1, 2c, 2e, 5, 6, S3 and S4) or Kruskal-Wallis
341 test followed by Tukey multiple comparison (Figures 2d, 3 and 4b). P-values of less than 0.05
342 were considered significant.
343

344 **References**

345 Arsenovic, P.T., Ramachandran, I., Bathula, K., Zhu, R., Narang, J.D., Noll, N.A., Lemmon, C.A.,
346 Gundersen, G.G., Conway, D.E., 2016. Nesprin-2G, a Component of the Nuclear LINC Complex,
347 Is Subject to Myosin-Dependent Tension. Biophysical journal 110, 34-43.

348 Balakrishnan, S., Mathad, S.S., Sharma, G., Raju, S.R., Reddy, U.B., Das, S., Ananthasuresh, G.K.,
349 2019. A Nondimensional Model Reveals Alterations in Nuclear Mechanics upon Hepatitis C
350 Virus Replication. Biophysical journal 116, 1328-1339.

351 Buxboim, A., Swift, J., Irianto, J., Spinler, K.R., Dingal, P.C., Athirasala, A., Kao, Y.R., Cho, S.,
352 Harada, T., Shin, J.W., Discher, D.E., 2014. Matrix elasticity regulates lamin-A,C phosphorylation
353 and turnover with feedback to actomyosin. Current biology : CB 24, 1909-1917.

354 Case, N., Xie, Z., Sen, B., Styner, M., Zou, M., O'Conor, C., Horowitz, M., Rubin, J., 2010.
355 Mechanical activation of β-catenin regulates phenotype in adult murine marrow-derived
356 mesenchymal stem cells. Journal of Orthopaedic Research 28, 1531-1538.

357 Chan, C.J., Li, W., Cojoc, G., Guck, J., 2017. Volume Transitions of Isolated Cell Nuclei Induced by
358 Rapid Temperature Increase. Biophysical journal 112, 1063-1076.

359 Crisp, M., Liu, Q., Roux, K., Rattner, J.B., Shanahan, C., Burke, B., Stahl, P.D., Hodzic, D., 2006.
360 Coupling of the nucleus and cytoplasm: role of the LINC complex. The Journal of Cell Biology
361 172, 41-53.

362 Guilluy, C., Osborne, L.D., Van Landeghem, L., Sharek, L., Superfine, R., Garcia-Mata, R.,
363 Burridge, K., 2014. Isolated nuclei adapt to force and reveal a mechanotransduction pathway in
364 the nucleus. Nature cell biology 16, 376-381.

365 Guo, Q., Xia, Y., Sandig, M., Yang, J., 2012. Characterization of cell elasticity correlated with cell
366 morphology by atomic force microscope. Journal of biomechanics 45, 304-309.
367 Hodzic, D.M., Yeater, D.B., Bengtsson, L., Otto, H., Stahl, P.D., 2004. Sun2 Is a Novel Mammalian
368 Inner Nuclear Membrane Protein. Journal of Biological Chemistry 279, 25805-25812.
369 Imai, R., Nozaki, T., Tani, T., Kaizu, K., Hibino, K., Ide, S., Tamura, S., Takahashi, K., Shribak, M.,
370 Maeshima, K., 2017. Density imaging of heterochromatin in live cells using orientation-
371 independent-DIC microscopy. Molecular biology of the cell 28, 3349-3359.
372 Khan, Z.S., Santos, J.M., Hussain, F., 2018. Aggressive prostate cancer cell nuclei have reduced
373 stiffness. Biomicrofluidics 12, 014102.
374 Lammerding, J., Fong, L.G., Ji, J.Y., Reue, K., Stewart, C.L., Young, S.G., Lee, R.T., 2006. Lamins A
375 and C but Not Lamin B1 Regulate Nuclear Mechanics. Journal of Biological Chemistry 281,
376 25768-25780.
377 Le, H.Q., Ghatak, S., Yeung, C.Y., Tellkamp, F., Gunschmann, C., Dieterich, C., Yeroslaviz, A.,
378 Habermann, B., Pombo, A., Niessen, C.M., Wickstrom, S.A., 2016. Mechanical regulation of
379 transcription controls Polycomb-mediated gene silencing during lineage commitment. Nature
380 cell biology 18, 864-875.
381 Lessey, E.C., Guilluy, C., Burridge, K., 2012. From mechanical force to RhoA activation.
382 Biochemistry 51, 7420-7432.
383 Lombardi, M.L., Jaalouk, D.E., Shanahan, C.M., Burke, B., Roux, K.J., Lammerding, J., 2011. The
384 Interaction between Nesprins and Sun Proteins at the Nuclear Envelope Is Critical for Force
385 Transmission between the Nucleus and Cytoskeleton. Journal of Biological Chemistry 286,
386 26743-26753.

387 Martins, R.P., Finan, J.D., Farshid, G., Lee, D.A., 2012. Mechanical Regulation of Nuclear
388 Structure and Function. Annual review of biomedical engineering 14, 431-455.
389 Matsumoto, A., Hieda, M., Yokoyama, Y., Nishioka, Y., Yoshidome, K., Tsujimoto, M., Matsuura,
390 N., 2015. Global loss of a nuclear lamina component, lamin A/C, and LINC complex components
391 SUN1, SUN2, and nesprin-2 in breast cancer. Cancer Med.
392 Miroshnikova, Y.A., Nava, M.M., Wickstrom, S.A., 2017. Emerging roles of mechanical forces in
393 chromatin regulation. Journal of cell science 130, 2243-2250.
394 Neelam, S., Chancellor, T.J., Li, Y., Nickerson, J.A., Roux, K.J., Dickinson, R.B., Lele, T.P., 2015.
395 Direct force probe reveals the mechanics of nuclear homeostasis in the mammalian cell.
396 Proceedings of the National Academy of Sciences of the United States of America 112, 5720-
397 5725.
398 Ozcivici, E., Luu, Y.K., Adler, B., Qin, Y.X., Rubin, J., Judex, S., Rubin, C.T., 2010. Mechanical
399 signals as anabolic agents in bone. Nature reviews. Rheumatology 6, 50-59.
400 Padmakumar, V.C., Libotte, T., Lu, W., Zaim, H., Abraham, S., Noegel, A.A., Gotzmann, J.,
401 Foisner, R., Karakesisoglou, I., 2005. The inner nuclear membrane protein Sun1 mediates the
402 anchorage of Nesprin-2 to the nuclear envelope. Journal of cell science 118, 3419-3430.
403 Pagnotti, G.M., Styner, M., Uzer, G., Patel, V.S., Wright, L.E., Ness, K.K., Guise, T.A., Rubin, J.,
404 Rubin, C.T., 2019. Combating osteoporosis and obesity with exercise: leveraging cell
405 mechanosensitivity. Nature Reviews Endocrinology.
406 Paine, P.L., Austerberry, C.F., Desjarlais, L.J., Horowitz, S.B., 1983. Protein loss during nuclear
407 isolation. J Cell Biol 97, 1240-1242.

408 Peister, A., Mellad, J.A., Larson, B.L., Hall, B.M., Gibson, L.F., Prockop, D.J., 2004. Adult stem
409 cells from bone marrow (MSCs) isolated from different strains of inbred mice vary in surface
410 epitopes, rates of proliferation, and differentiation potential. Blood 103, 1662-1668.
411 Pongkitwitoon, S., Uzer, G., Rubin, J., Judex, S., 2016. Cytoskeletal Configuration Modulates
412 Mechanically Induced Changes in Mesenchymal Stem Cell Osteogenesis, Morphology, and
413 Stiffness. Scientific reports 6, 34791.
414 Rando, T.A., Ambrosio, F., 2018. Regenerative Rehabilitation: Applied Biophysics Meets Stem
415 Cell Therapeutics. Cell Stem Cell 22, 306-309.
416 Rubin, J., Styner, M., Uzer, G., 2018. Physical Signals May Affect Mesenchymal Stem Cell
417 Differentiation via Epigenetic Controls. Exercise and sport sciences reviews 46, 42-47.
418 Sen, B., Xie, Z., Case, N., Styner, M., Rubin, C.T., Rubin, J., 2011. Mechanical signal influence on
419 mesenchymal stem cell fate is enhanced by incorporation of refractory periods into the loading
420 regimen. Journal of biomechanics 44, 593-599.
421 Stephens, A.D., Banigan, E.J., Adam, S.A., Goldman, R.D., Marko, J.F., 2017. Chromatin and
422 lamin A determine two different mechanical response regimes of the cell nucleus. Molecular
423 biology of the cell 28, 1984-1996.
424 Stephens, A.D., Liu, P.Z., Banigan, E.J., Almassalha, L.M., Backman, V., Adam, S.A., Goldman,
425 R.D., Marko, J.F., 2018. Chromatin histone modifications and rigidity affect nuclear morphology
426 independent of lamins. Molecular biology of the cell 29, 220-233.
427 Swift, J., Ivanovska, I.L., Buxboim, A., Harada, T., Dingal, P.C.D.P., Pinter, J., Pajerowski, J.D.,
428 Spinler, K.R., Shin, J.-W., Tewari, M., Rehfeldt, F., Speicher, D.W., Discher, D.E., 2013. Nuclear

429 Lamin-A Scales with Tissue Stiffness and Enhances Matrix-Directed Differentiation. Science
430 (New York, N.Y.) 341.
431 Uzer, G., Bas, G., Sen, B., Xie, Z., Birks, S., Olcum, M., McGrath, C., Styner, M., Rubin, J., 2018.
432 Sun-mediated mechanical LINC between nucleus and cytoskeleton regulates betacatenin
433 nuclear access. J Biomech 74, 32-40.
434 Uzer, G., Pongkitwitoon, S., Ete Chan, M., Judex, S., 2013. Vibration induced osteogenic
435 commitment of mesenchymal stem cells is enhanced by cytoskeletal remodeling but not fluid
436 shear. Journal of Biomechanics 46, 2296-2302.
437 Uzer, G., Thompson, W.R., Sen, B., Xie, Z., Yen, S.S., Miller, S., Bas, G., Styner, M., Rubin, C.T.,
438 Judex, S., Burridge, K., Rubin, J., 2015. Cell Mechanosensitivity to Extremely Low-Magnitude
439 Signals Is Enabled by a LINCed Nucleus. STEM CELLS 33, 2063-2076.
440 Versaevel, M., Braquenier, J.-B., Riaz, M., Grevesse, T., Lantoine, J., Gabriele, S., 2014. Super-
441 resolution microscopy reveals LINC complex recruitment at nuclear indentation sites. Sci. Rep.
442 4.
443

444 **Figure Legends**

445 **Figure 1. Nuclear geometry characteristics before and after nuclear isolation. a)**
446 Mesenchymal stem cells (top) and isolated nuclei (bottom) were stained with Hoechst 33342
447 and subsequently imaged for DNA using a fluorescence microscope. **b)** Confocal imaging of an
448 intact nucleus (top) and isolated nucleus (bottom) with Hoechst 33342 fluorescence staining
449 under 63x focus with 16 Z-stacks for each nucleus image. Representative intact MSC (top) and
450 isolated nucleus (bottom) shown in XY, XZ, and YZ planes of focus. Staining against LaminA/C

451 also indicated an intact nuclear lamina post-isolation. **c)** Shape profiles of the intact MSC nuclei
452 versus isolated nuclei. The isolated and intact nuclei exhibited similar circularity in the XY plane
453 (i.e., the horizontal plane of the cell culture dish or microscope slide), but showed significant
454 differences in shape profiles in the vertical XZ and YZ planes ($p<.001$, N=10 isolated nuclei, N=10
455 intact nuclei), with isolated nuclei showing 52% and 45% higher circularity values in those
456 planes, respectively. The combined data, which is an average of all three planes, shows a
457 significant difference in sphericity ($p<.001$) between the isolated nuclei and intact nuclei, with
458 the two types having sphericity values of 0.809 and 0.612, respectively. **d)** Average isolated
459 nuclear height (9.43 µm) is approximately twice that of intact MSC nuclei (4.59 µm,
460 N=10/group, $p<.001$). e) Volume decreases from 1,116 μm^3 to 621 μm^3 following isolation
461 (N=10/group, $p<.001$. * $p<.05$, ** $p<.01$, *** $p<.001$, against control.
462
463 **Figure 2. Nucleus significantly contributes to AFM-measured MSC stiffness. a)** Nuclear
464 isolation protocol involved plating of nuclei onto a 35 mm cell culture dish coated in poly-L-
465 lysine. Isolated nuclei were incubated for 25 minutes at 37˚C with 1 mL 1X PBS to ensure
466 adhesion to the substrate immediately prior to AFM testing for up to 1 hour. Shown are both
467 cartoons and actual optical images of intact MSCs and isolated nuclei as seen in the AFM
468 camera. **b)** SEM image of a Bruker MLCT-D tipless AFM cantilever with a 10 µm diameter glass
469 bead standard (Thermo Scientific 9010) attached. Scale bars were 30 µm (bottom image) and
470 10 µm (top image). **c)** Fixation of isolated nuclei in 2% paraformaldehyde (2% PFA) for 10
471 minutes showed an almost 4-fold increase in modulus compared to live controls ($p<.01$,
472 N=10/grp). **d)** AFM measurements show no change in the elastic modulus of isolated nuclei

473 over a 2-hour testing interval, after 2-hour window there was a 405% increase in the nuclear
474 stiffness (p<.01). **e)** Isolated nuclei were identified via AFM and tested in the center of the
475 nucleus to collect three individual measurements per sample. Intact MSCs and Isolated nuclei
476 (both live) were plated on 35 mm dishes and tested for stiffness via AFM for one-hour intervals.
477 The cell nucleus accounts for 69.7% of the total measured MSC stiffness with a modulus of 1.51
478 kPa (N=119). For comparison, the average stiffness of MSCs (passage 8-11) was 2.19 kPa
479 (N=124). * p<.05, ** p<.01, *** p<.001, against control or against each other.
480
481 **Figure 3. Disruption of LaminA/C decreases nuclear stiffness and changes structure. a)**
482 Schematic representation of the nucleus with nucleoskeletal and cytoskeletal connection
483 components illustrated, including LaminA/C, Sun-1&2, Nesprin, and the KASH domain. **b)** SiRNA
484 against nuclear LaminA/C (siLmn) and Sun-1&2 (siSun) decreased both isolated nuclear and
485 intact MSC stiffness. Compared to siCtrl (N=21), siLmn and siSun treatments showed a
486 significant decrease in the intact MSC modulus by 63.2% (p<.05, N=22) and 50.7% (p>.05,
487 N=10), respectively. Likewise, when compared to siCtrl (N=21) the elastic modulus of isolated
488 nuclei decreased by 49.7% (p<.01, N=21) and 27.7% (p>.05 N=10) in siLmn and siSun groups,
489 respectively. **c)** A MATLAB code was constructed to evaluate differences in nuclear area and
490 nucleoli size as determined by live Hoechst 33342 staining (see Supplementary Methods). **d)**
491 Nuclear staining via Hoechst 33342 and epifluorescence imaging revealed that nuclear area
492 increased by 33% within siLmn treated intact MSCs (p<.001, N=73), but not under Sun-1&2
493 depletion when compared to siCtrl (N=104). Nuclear area showed no significant changes within
494 isolated nuclei control or experimental groups (N=245). **e)** Chromatin area to nuclear area

495 ratios were calculated for all MSC and isolated nuclei for siCtrl, siLmn and siSun groups.
496 Compared to controls (N=806), intact MSC did not show differences in chromatin to nuclear
497 area ratio for LaminA/C (N=647) andSun-1&2 MSCs (N=489). In contrast, isolated nuclei showed
498 significant increases in chromatin to nuclear area ratios for both LaminA/C (47.2%, p<.001,
499 N=502) and Sun-1&2 (39.1%, p<.001, N=612) depleted nuclei compared to controls (N=416). *
500 p<.05, ** p<.01, *** p<.001, against control or against each other.
501
502 **Figure 4. LIV stiffens intact MSCs and isolated nuclei. a**) Low intensity vibration (0.7g, 90 Hz)
503 was applied to MSCs at twenty-minute intervals with one-hour rest in between each vibration
504 bout. 2x vibration included two, twenty-minute vibration periods, while 4x included four
505 periods. **b)** In intact MSCs, 2x LIV increased AFM-measured elastic modulus on MSCs by 71%
506 (N=31, p<.05). 4x LIV resulted in 419% increase in elastic modulus (N=33, p<.001) compared to
507 control (N=32). **c)** Nuclear response to LIV was measured by applying the 2x LIV protocol to
508 intact MSCs and then isolating nuclei to test stiffness. 2x LIV showed no significant increase in
509 stiffness in comparison to control (N=20). Nuclei responded to 4x LIV by showing a 75%
510 increase in modulus (N=24, p<0.05) when compared to control nuclei (N=27) post-LIV isolation.
511 **d)** Western blotting for LaminA/C and Sun-2 show no changes in protein levels for 4x LIV groups
512 compared to their respective controls (N=3/grp). * p<.05, ** p<.01, *** p<.001, against control
513 or against each other.
514
515 **Figure 5. Isolated nuclei maintain heterochromatin area after vibration. a)** Epi-fluorescence
516 images of intact control MSC nuclei (upper left), intact 4x LIV MSC nuclei (lower left), isolated

517 control nuclei (upper right), and isolated 4x LIV nuclei (lower right). Cells were treated with
518 Hoechst 33342 to stain heterochromatin, fixed in 2% paraformaldehyde, and kept in PBS for
519 imaging. **b)** Nuclear area was measured using MATLAB code to identify nuclear bounds under
520 Hoechst 33342 staining. Intact MSCs subject to 4x LIV (N=216) showed no difference in nuclear
521 area compared to controls (N=214). Likewise, there was no difference in nuclear area between
522 control (N=90) and 4x LIV isolated nuclei (N=102). **c)** Chromatin measurements were analyzed
523 via MATLAB analysis. Individual chromatin were averaged and compared to respective nuclear
524 area. Intact MSCs subject to 4x LIV (N=2136) showed no difference in chromatin to nuclear area
525 ratio compared to controls (N=2082). Isolated nuclei subject to 4x LIV showed a 25.4% lower
526 chromatin to nuclear area ratio (N=480) than isolated controls (p<.05, N=360). * p<.05, **
527 p<.01, *** p<.001, against control.
528
529 **Figure 6. LINC function is required for LIV-induced nuclear stiffening. a)** Overexpressing
530 dominant negative form of Nesprin KASH domain was used to disrupt LINC function in MSCs. **b)**
531 Intact MSCs and **c)** isolated nuclei did not show any response to 4x LIV (N=20/grp). * p<.05, **
532 p<.01, *** p<.001, against control.
533
534 **APPENDIX: Supplementary Figure Legends & Tables and Methods**
535
536 **Supplementary Figure Legends**
537 **Figure S1.** Nuclei were either left intact inside MSCs or isolated (isolation protocol, methods),
538 stained with Hoechst 33342, and fixed in 2% paraformaldehyde. As shown in these videos, a

539 Leica 6500 confocal microscope was then used to acquire vertical stacked images of both nuclei
540 inside intact MSC samples (left) and isolated nuclei (right).
541
542 **Fig. S2 a)** SEM image of a Bruker MLCT-D AFM probe functionalized with a 10 µm diameter glass
543 bead (Thermo Scientific 9010 NIST-traceable 9000 Series Glass Particle Standard, 10.0 ± 1.0
544 µm). **b)** Representative thermal tune of an MLCT-D probe functionalized with such a 10 µm
545 glass bead. Nominal resonance frequency of the MLCT-D cantilever prior to bead
546 functionalization is 10-20 kHz, with the added weight of the bead causing the resonance to shift
547 to lower frequency. A simple harmonic oscillator fit was used (red) to model the resonant
548 response of the cantilever in a fluid environment. **c)** Representative ramp data. Ramping to a
549 maximum excursion/extension of 1 µm was performed at a rate of 1 Hz (i.e., 2 µm/sec
550 load/unload velocity).
551
552 **Fig S3.** Compared to empty control plasmid (pCDH-EF1-MSC1-puro-mCherry), LINC-disrupted
553 intact cells (N=10/grp) and isolated nuclei (N=20/grp) did not show any changes in stiffness. *
554 p<.05, ** p<.01, *** p<.001, against control.
555
556 **Figure S4.** MSCs measured via AFM-based nanoindentation showed 132% higher elastic
557 modulus in passage 15 samples (P15, N=10, p<.001) compared to samples between passages 8
558 and 11 (P8-11, N=45). * p<.05, ** p<.01, *** p<.001, against control or against each other.
559

560 **Figure S5.** Unprocessed blots as obtained by LiCor C-DiGit blot scanner. Red lines outline the
561 representative blots used.
562
563 **Supplementary Methods**
564 Overexpression and Small Interfering RNA (siRNA)
565 PCDH-EF1-MCS1-puro-mCherry (mCherry control) and pCDH-EF1-MCS1-puro-mCherry-Nesprin-
566 1αKASH plasmids were kindly provided by Dr. Lammerding. mdMSCs were transfected using
567 1µg DNA per 100,000 cells using LipoD293 transfection reagent (SignaGen Laboratories,
568 Rockville, MD) according to the manufacturer's instructions. 72 hr after the initial transfection,
569 stably transfected cells were selected using 10 µg/ml puromycin. For transiently silencing
570 specific genes, cells were transfected with gene-specific small interfering RNA (siRNA) or control
571 siRNA (20 nM) using PepMute Plus transfection reagent (SignaGen Labs) according to the
572 manufacturer's instructions. The following siRNAs were used in this study: negative control for
573 SUN-1 5'- GAAATCGAAGTACCTCGAGTGATAT -3'; SUN-1 5'- GAAAGGCTATGAATCCAGAGCTTAT-
574 3'; negative control for SUN-2 5'-CACCAGAGGCTAGAACTCTTACTCA-3'; SUN-2 5'-
575 CAACAUCCCUCAUGGGCCUAUUGUG-3'. '; negative control for LaminA/C 5'-
576 UGGGAGUCGGAAGAAGACUCGAUCA-3'; LaminA/C 5'-UGGGAGAGGCUAAGAAGCAGCUUCA-3'.
577
578 Western Blotting
579 We used previously established western blot protocols (Uzer et al., 2018). Briefly, 20 µg of
580 protein from each sample was separated on 9% polyacrylamide gels and transferred to
581 polyvinylidene difluoride (PVDF) membranes. Membranes were blocked with 5% milk (w/v in

582 TBST-T) and incubated overnight at 4˚C with a specific primary antibody. Next, blots were
583 washed and incubated with horseradish peroxidase-conjugated secondary antibody diluted at
584 1:5,000 (Cell Signaling) at room temperature for 1 hr. An ECL plus (Amersham Biosciences,
585 Piscataway, NJ) kit and LiCor C-DiGit scanner were used to obtain quantitative data.
586 Densitometry analysis was performed via NIH ImageJ using at least three independent
587 experiments. During densitometry, each protein of interest was normalized to GAPDH or PARP,
588 which were used as housekeeping proteins for whole cell or nuclear fractions, respectively. A
589 list of primary antibodies used is given in **Table S2**.
590
591 Immunofluorescence and Image Analysis
592 Prior to experiments, nuclei were stained with Hoechst 33342 vital dye (Nucblue,
593 ThermoFisher) according to the manufacturer instructions. Following the LIV protocol, intact
594 MSCs or isolated live nuclei were fixed with 2% paraformaldehyde for 15 minutes. For
595 chromatin intensity analysis, nuclei were imaged using an epifluorescence microscope (Revolve,
596 Echo Labs). Chromatin intensity analyses were performed using a custom MATLAB script to
597 select regions of nuclei. Hoechst stain was used to define the nuclear regions through the use of
598 the blue channel. Each nucleus was individually defined, along with its intensity converted to 8-
599 bit (i.e., a brightness range of 0-255). The mean brightness intensity of each nucleus was
600 computed with heterochromatin being defined as +35 intensity relative to the average. The rest
601 of the nuclear area was defined as non-heterochromatin, with the chromatin area and centroid
602 then reported as output.
603

604 A heterochromatin area to nuclear area ratio was calculated to estimate average
605 heterochromatin size as an indicator for changes in chromatin condensation. Individual
606 heterochromatin regions were identified in isolated and intact nuclei for siRNA samples and
607 vibrated samples using the previously described MATLAB technique. The ratio between
608 heterochromatin average area and average nuclear area was computed and groups were
609 compared using independent t-tests.
610
611 To quantify the nuclear geometry, the entire height of individual cells or nuclei were identified
612 and further imaged using a Leica 6500 confocal microscope, which evenly divided each sample
613 into sixteen vertical stacks **(Fig. S1**). Confocal image stacks were imported into FIJI ImageJ
614 software (https://imagej.nih.gov/ij/). Using Hoechst 33342 as a landmark, nuclear height was
615 quantified via counting the number of stacks between first and last slices with detectable, in-
616 focus Hoechst 33342 signal using cross-sectional images. Next, the entire nuclear section was
617 collapsed into a single image using "Average Intensity Projection." Nuclear area was measured
618 via tracing the outer circumference of Hoechst 33342. This allowed for the perimeter in each of
619 the three planes of measurement (XY, XZ, and YZ) to be identified. From there, the "circularity"
620 tool was used to compare each perimeter to that of a perfect circle. Averages for each plane of
621 individual images were computed in Microsoft Excel for the two groups: intact MSC nuclei and
622 isolated nuclei. The circularity values for each plane were then averaged to obtain a sphericity
623 value for the two groups of nuclei.
624
625 **Supplementary Tables**

626 **Table.S1:** Cell culture and pharmacological reagents

Cell Culture and Pharmacological Reagents		Final Concentration
IMDM	GIBCO	-
Fetal Calf Serum (FCS)	Atlanta Biologicals	10% v/v
Penicillin/streptomycin	GIBCO	1% v/v
SB415286	Sigma Aldrich	20µM

627

628 **Table.S2:** Antibodies and concentrations

Antibodies		Final Concentration
PARP (9542T)	Cell Signaling	1/1000
GAPDH (5174S)	Cell Signaling	1/1000
LaminA/C (#4C11)	Cell Signaling	1/1000
Sun-2 (ab87036)	Abcam	1/1000

629

630 **Table.S3:** Immunostaining antibodies, reagents, and concentrations

Immunostaining Antibodies and Reagents		Final Concentration
Alexa Flour 555 Donkey Anti-Rabbit	Invitrogen	1/500
Hoechst 33342	Invitrogen	1 µg/mL
LaminA/C (#4C11)	Cell Signaling	1/300

631

632 **Table.S4:** Overexpression reagents and concentrations

Knockdown and Overexpression Reagents		Final Concentration
LipoD293	SignaGen Laboratories	3µL per mL
PepMute Plus	SignaGen Laboratories	3µL per µg of DNA
Puromycin	Sigma Aldrich	10 µg/mL

633

Figure 1

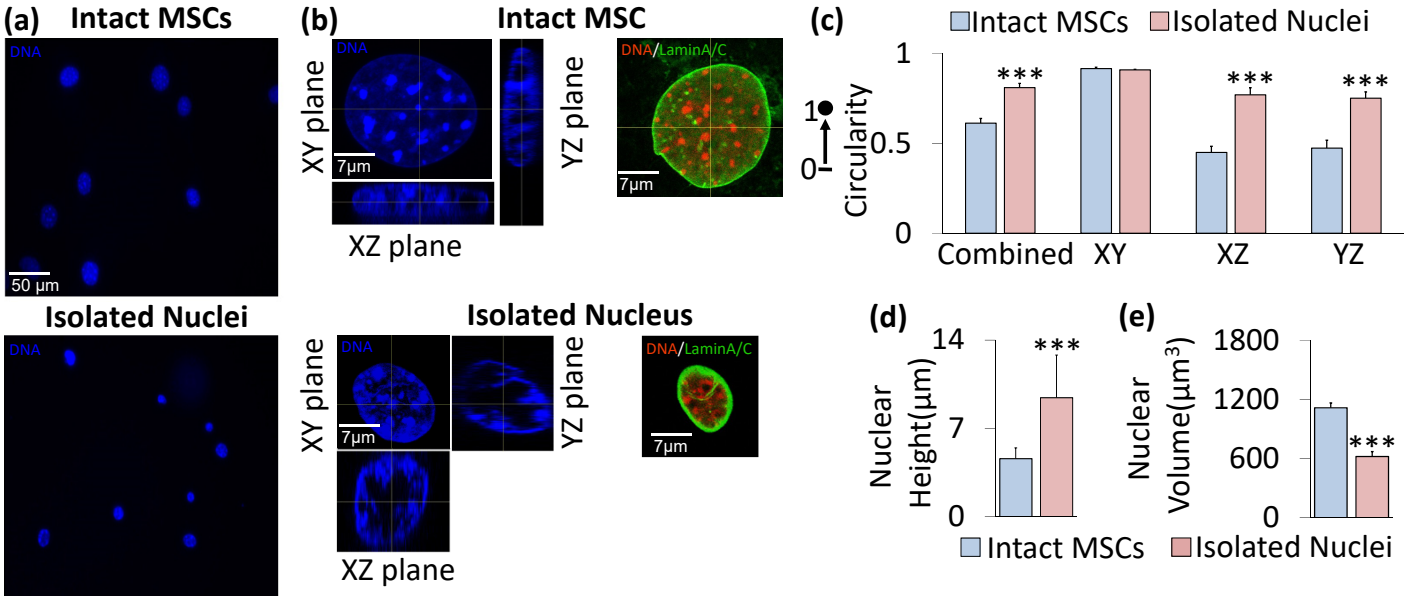

Figure 1. Nuclear geometry characteristics before and after nuclear isolation. a) Mesenchymal stem cells (top) and isolated nuclei (bottom) were stained with Hoechst 33342 and subsequently imaged for DNA using a fluorescence microscope. **b)** Confocal imaging of an intact nucleus (top) and isolated nucleus (bottom) with Hoechst 33342 fluorescence staining under 63x focus with 16 Z-stacks for each nucleus image. Representative intact MSC (top) and isolated nucleus (bottom) shown in XY, XZ, and YZ planes of focus. Staining against LaminA/C also indicated an intact nuclear lamina post-isolation. **c)** Shape profiles of the intact MSC nuclei versus isolated nuclei. The isolated and intact nuclei exhibited similar circularity in the XY plane (i.e., the horizontal plane of the cell culture dish or microscope slide), but showed significant differences in shape profiles in the vertical XZ and YZ planes ($p<.001$, N=10 isolated nuclei, N=10 intact nuclei), with isolated nuclei showing 52% and 45% higher circularity values in those planes, respectively. The combined data, which is an average of all three planes, shows a significant difference in sphericity ($p<.001$) between the isolated nuclei and intact nuclei, with the two types having sphericity values of 0.809 and 0.612, respectively. **d)** Average isolated nuclear height (9.43 µm) is approximately twice that of intact MSC nuclei (4.59 µm, N=10/group, $p<.001$). **e)** Volume decreases from 1,116 μm^3 to 621 μm^3 following isolation (N=10/group, $p<.001$. * $p<.05$, ** $p<.01$, *** $p<.001$, against control.

Figure 2

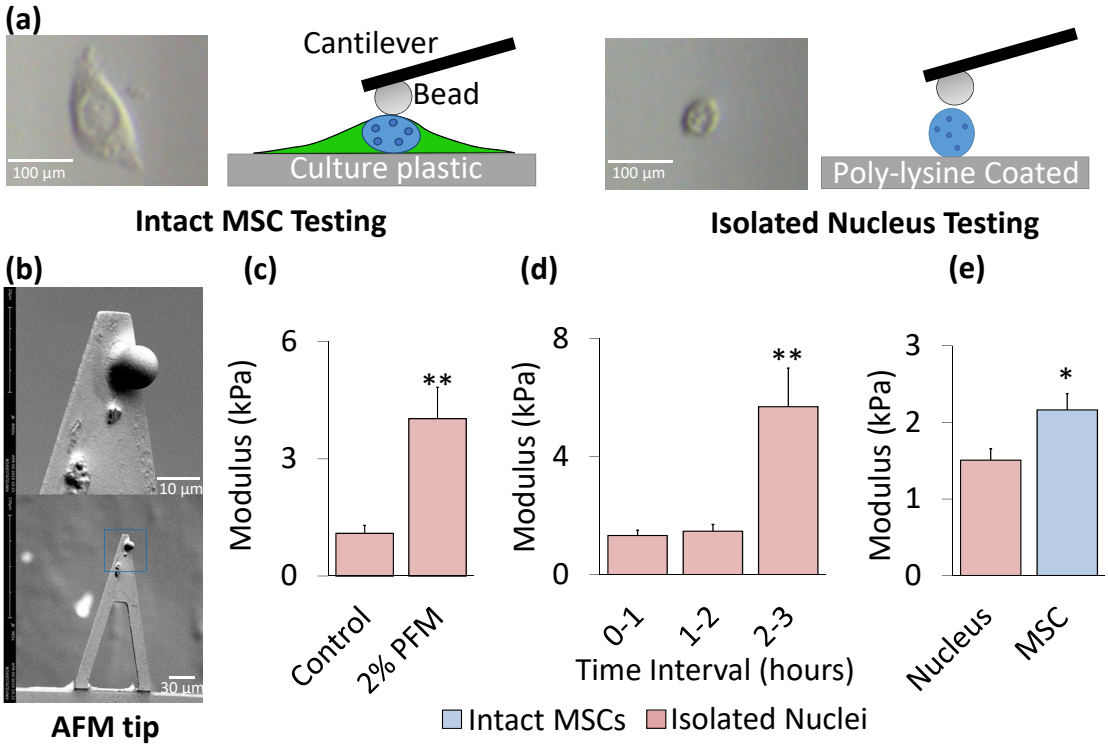

Figure 2. Nucleus significantly contributes to AFM-measured MSC stiffness. a) Nuclear isolation protocol involved plating of nuclei onto a 35 mm cell culture dish coated in poly-L-lysine. Isolated nuclei were incubated for 25 minutes at 37˚C with 1 mL 1X PBS to ensure adhesion to the substrate immediately prior to AFM testing for up to 1 hour. Shown are both cartoons and actual optical images of intact MSCs and isolated nuclei as seen in the AFM camera. **b)** SEM image of a Bruker MLCT-D tipless AFM cantilever with a 10 µm diameter glass bead standard (Thermo Scientific 9010) attached. Scale bars were 30 µm (bottom image) and 10 µm (top image). **c)** Fixation of isolated nuclei in 2% paraformaldehyde (2% PFA) for 10 minutes showed an almost 4-fold increase in modulus compared to live controls ($p<.01$, N=10/grp). **d)** AFM measurements show no change in the elastic modulus of isolated nuclei over a 2-hour testing interval, after 2-hour window there was a 405% increase in the nuclear stiffness ($p<.01$). **e)** Isolated nuclei were identified via AFM and tested in the center of the nucleus to collect three individual measurements per sample. Intact MSCs and Isolated nuclei (both live) were plated on 35 mm dishes and tested for stiffness via AFM for one-hour intervals. The cell nucleus accounts for 69.7% of the total measured MSC stiffness with a modulus of 1.51 kPa (N=119). For comparison, the average stiffness of MSCs (passage 8-11) was 2.19 kPa (N=124). * $p<.05$, ** $p<.01$, *** $p<.001$, against control or against each other.

Figure 3

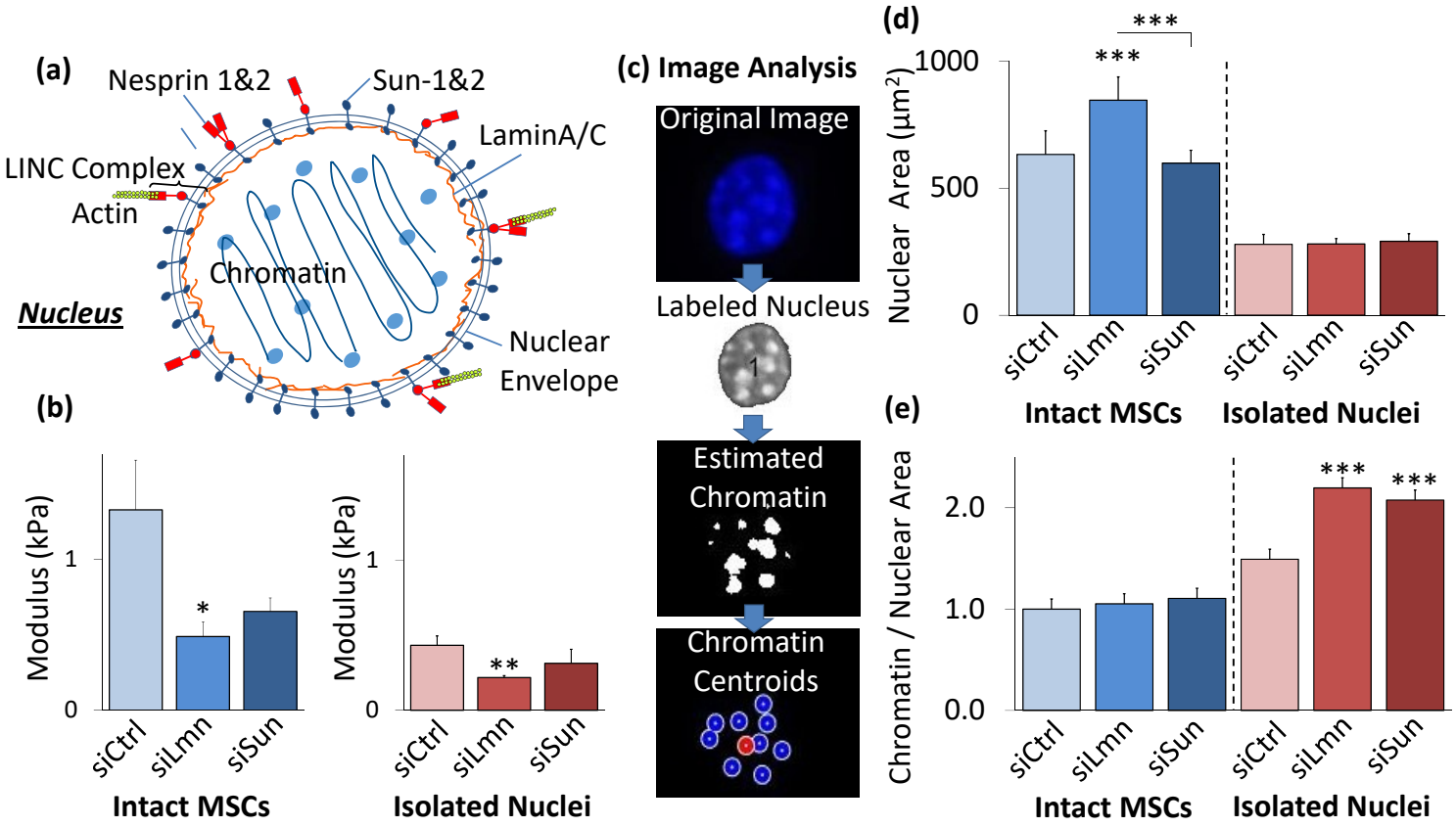

Figure 3. Disruption of LaminA/C decreases nuclear stiffness and changes structure. **a)** Schematic representation of the nucleus with nucleoskeletal and cytoskeletal connection components illustrated, including LaminA/C, Sun-1&2, Nesprin, and the KASH domain. **b)** SiRNA against nuclear LaminA/C (siLmn) and Sun-1&2 (siSun) decreased both isolated nuclear and intact MSC stiffness. Compared to siCtrl (N=21), siLmn and siSun treatments showed a significant decrease in the intact MSC modulus by 63.2% ($p<.05$, N=22) and 50.7% ($p>.05$, N=10), respectively. Likewise, when compared to siCtrl (N=21) the elastic modulus of isolated nuclei decreased by 49.7% ($p<.01$, N=21) and 27.7% ($p>.05$ N=10) in siLmn and siSun groups, respectively. **c)** A MATLAB code was constructed to evaluate differences in nuclear area and nucleoli size as determined by live Hoechst 33342 staining (see Supplementary Methods). **d)** Nuclear staining via Hoechst 33342 and epifluorescence imaging revealed that nuclear area increased by 33% within siLmn treated intact MSCs ($p<.001$, N=73), but not under Sun-1&2 depletion when compared to siCtrl (N=104). Nuclear area showed no significant changes within isolated nuclei control or experimental groups (N=245). **e)** Chromatin area to nuclear area ratios were calculated for all MSC and isolated nuclei for siCtrl, siLmn and siSun groups. Compared to controls (N=806), intact MSC did not show differences in chromatin to nuclear area ratio for LaminA/C (N=647) andSun-1&2 MSCs (N=489). In contrast, isolated nuclei showed significant increases in chromatin to nuclear area ratios for both LaminA/C (47.2%, $p<.001$, N=502) and Sun-1&2 (39.1%, $p<.001$, N=612) depleted nuclei compared to controls (N=416). * $p<.05$, ** $p<.01$, *** $p<.001$, against control or against each other.

Figure 4

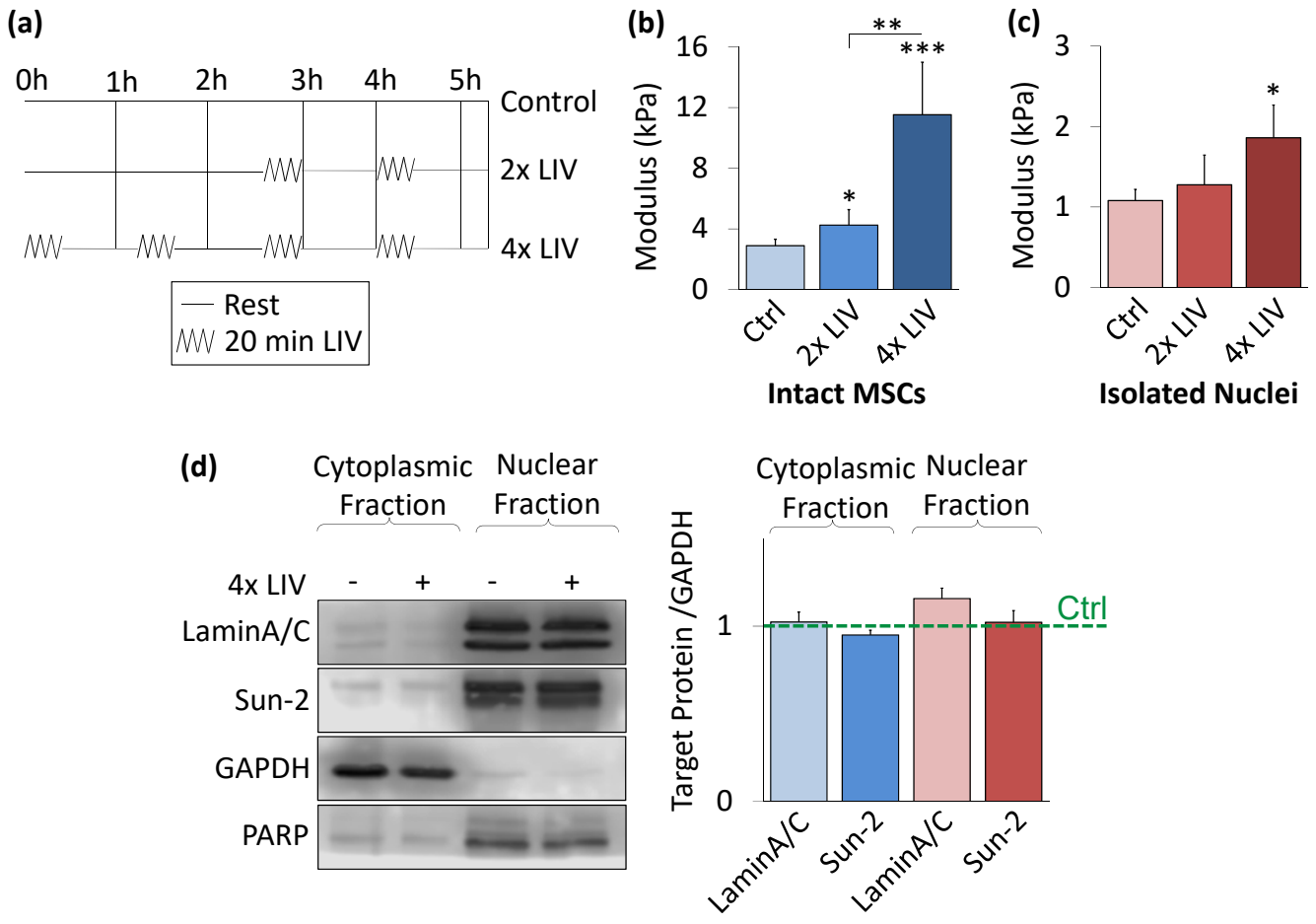

Figure 4. LIV stiffens intact MSCs and isolated nuclei. a) Low intensity vibration (0.7g, 90 Hz) was applied to MSCs at twenty-minute intervals with one-hour rest in between each vibration bout. 2x vibration included two, twenty-minute vibration periods, while 4x included four periods. **b)** In intact MSCs, 2x LIV increased AFM-measured elastic modulus on MSCs by 71% (N=31, p<.05). 4x LIV resulted in 419% increase in elastic modulus (N=33, p<.001) compared to control (N=32). **c)** Nuclear response to LIV was measured by applying the 2x LIV protocol to intact MSCs and then isolating nuclei to test stiffness. 2x LIV showed no significant increase in stiffness in comparison to control (N=20). Nuclei responded to 4x LIV by showing a 75% increase in modulus (N=24, p<0.05) when compared to control nuclei (N=27) post-LIV isolation. **d)** Western blotting for LaminA/C and Sun-2 show no changes in protein levels for 4x LIV groups compared to their respective controls (N=3/grp). * p<.05, ** p<.01, *** p<.001, against control or against each other.

Figure 5

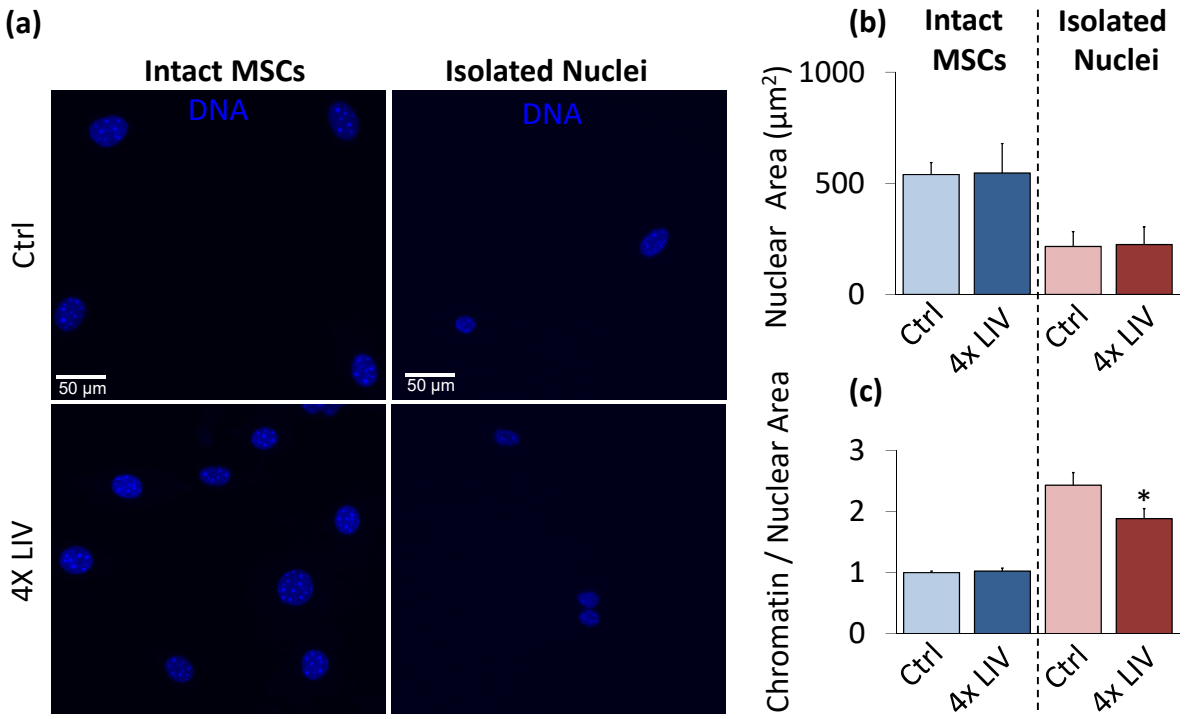

Figure 5. Isolated nuclei maintain heterochromatin area after vibration. a) Epi-fluorescence images of intact control MSC nuclei (upper left), intact 4x LIV MSC nuclei (lower left), isolated control nuclei (upper right), and isolated 4x LIV nuclei (lower right). Cells were treated with Hoechst 33342 to stain heterochromatin, fixed in 2% paraformaldehyde, and kept in PBS for imaging. **b)** Nuclear area was measured using MATLAB code to identify nuclear bounds under Hoechst 33342 staining. Intact MSCs subject to 4x LIV (N=216) showed no difference in nuclear area compared to controls (N=214). Likewise, there was no difference in nuclear area between control (N=90) and 4x LIV isolated nuclei (N=102). **c)** Chromatin measurements were analyzed via MATLAB analysis. Individual chromatin were averaged and compared to respective nuclear area. Intact MSCs subject to 4x LIV (N=2136) showed no difference in chromatin to nuclear area ratio compared to controls (N=2082). Isolated nuclei subject to 4x LIV showed a 25.4% lower chromatin to nuclear area ratio (N=480) than isolated controls ($p<.05$, N=360). * $p<.05$, ** $p<.01$, *** $p<.001$, against control.

Figure 5

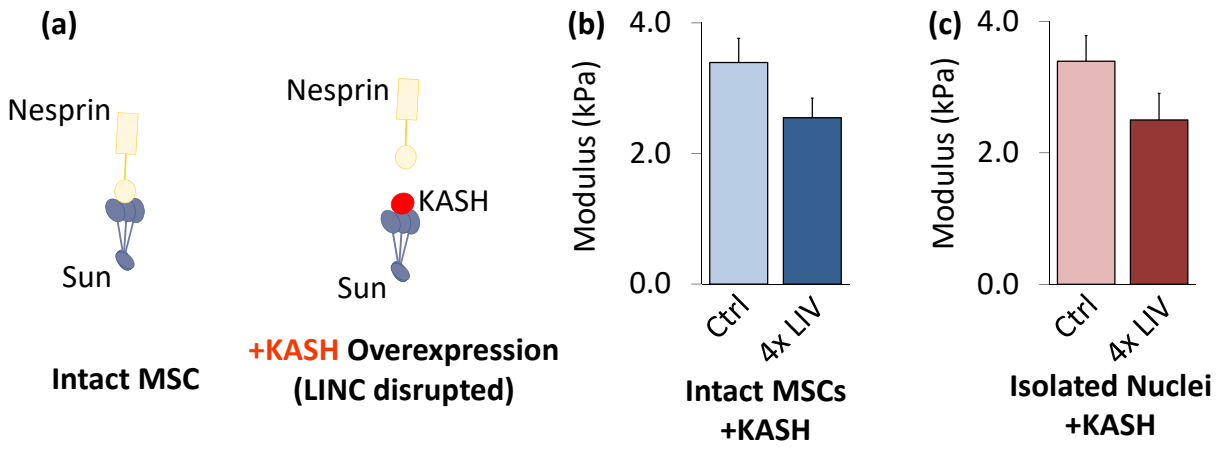

Figure 6. LINC function is required for LIV-induced nuclear stiffening. a) Overexpressing dominant negative form of Nesprin KASH domain was used to disrupt LINC function in MSCs. **b)** Intact MSCs and **c)** isolated nuclei did not show any response to 4x LIV (N=20/grp). * p<.05, ** p<.01, *** p<.001, against control.

Supplementary Information

Isolated Nuclei Stiffen in Response to Low Intensity Vibration

Newberg J[1], Schimpf J[2], Woods K[1], Loisate S[1], Davis P H[2], Uzer G[1] †

[1]Mechanical and Biomedical Engineering, Boise State University
[2]Micron School of Material Science, Boise State University
† Corresponding Author

Funding support: NIH R01AG059923, and 5P2CHD086843-03, P20GM109095, P20GM103408, NSF 1929188 and NASA ISGC NNX15AI04H.

Figure S1

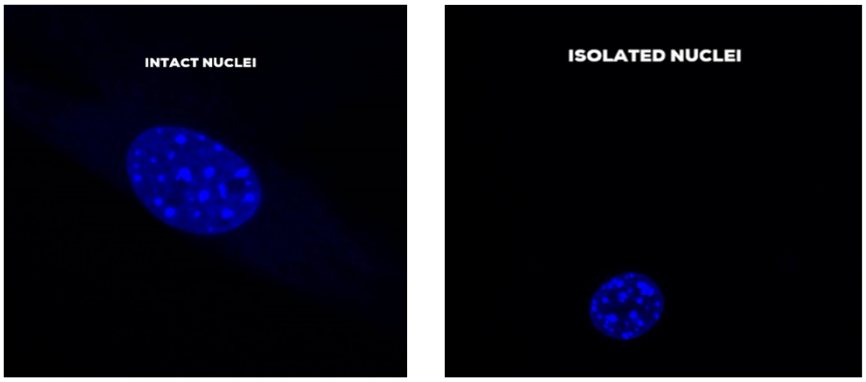

Figure S1. Nuclei were either left intact inside MSCs or isolated (isolation protocol, methods), stained with Hoechst 33342, and fixed in 2% paraformaldehyde. As shown in these videos, a Leica 6500 confocal microscope was then used to acquire vertical stacked images of both nuclei inside intact MSC samples (left) and isolated nuclei (right).

Figure S2

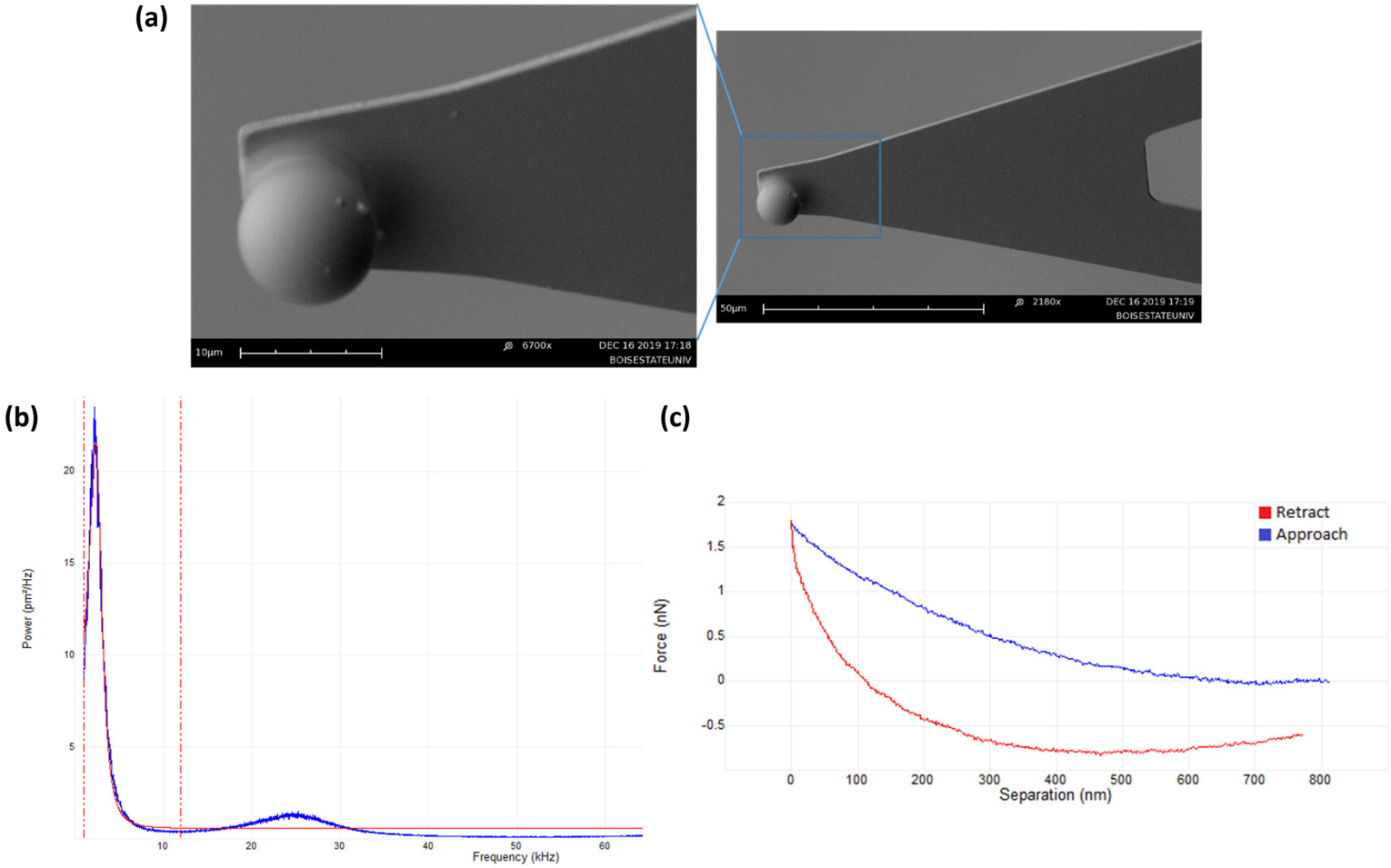

Fig. S2 a) SEM image of a Bruker MLCT-D AFM probe functionalized with a 10 µm diameter glass bead (Thermo Scientific 9010 NIST-traceable 9000 Series Glass Particle Standard, 10.0 ± 1.0 µm). **b)** Representative thermal tune of an MLCT-D probe functionalized with such a 10 µm glass bead. Nominal resonance frequency of the MLCT-D cantilever prior to bead functionalization is 10-20 kHz, with the added weight of the bead causing the resonance to shift to lower frequency. A simple harmonic oscillator fit was used (red) to model the resonant response of the cantilever in a fluid environment. **c)** Representative ramp data. Ramping to a maximum excursion/extension of 1 µm was performed at a rate of 1 Hz (i.e., 2 µm/sec load/unload velocity).

Figure S3

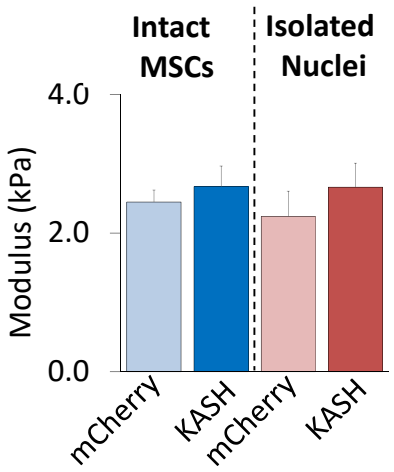

Fig S3. Compared to empty control plasmid (pCDH-EF1-MSC1-puro-mCherry), LINC-disrupted intact cells (N=10/grp) and isolated nuclei (N=20/grp) did not show any changes in stiffness. * p<.05, ** p<.01, *** p<.001, against control.

Figure S4

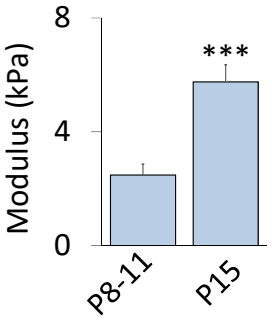

Figure S4. MSCs measured via AFM-based nanoindentation showed 132% higher elastic modulus in passage 15 samples (P15, N=10, p<.001) compared to samples between passages 8 and 11 (P8-11, N=45). * p<.05, ** p<.01, *** p<.001, against control or against each other.

Figure S5

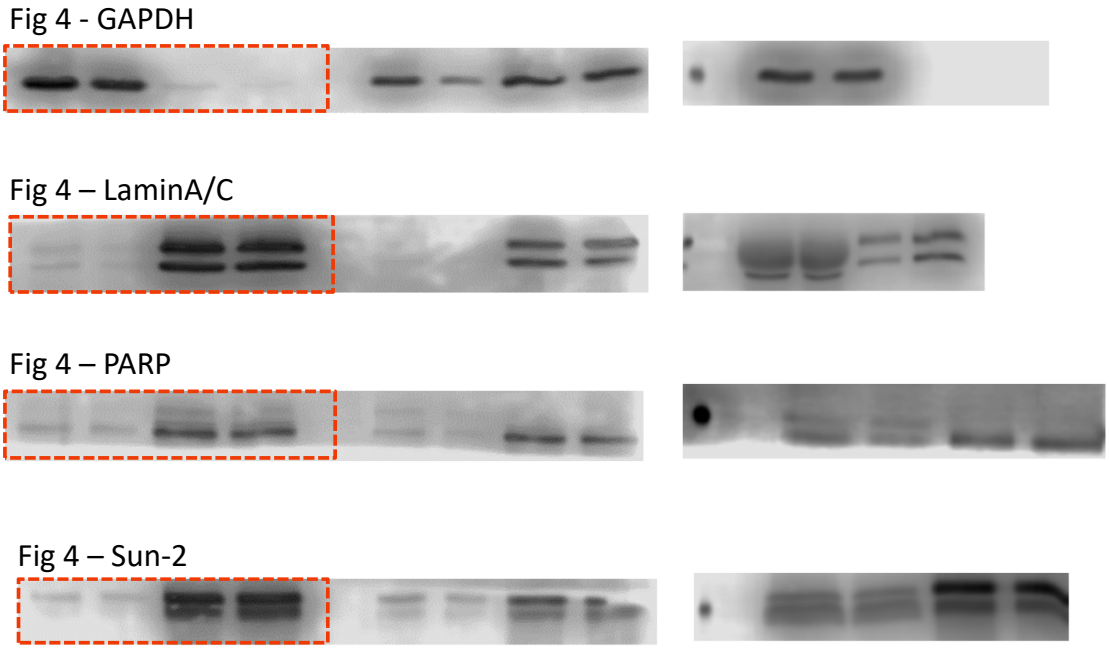

Figure S5. Unprocessed blots as obtained by LiCor C-DiGit blot scanner. Red lines outline the representative blots used.